J. Phycol. *, ***–*** (2020)

DOI: 10.1111/jpy.13017-20-020

INFLUENCE OF TEMPERATURE AND CO_2 ON PLASMA-MEMBRANE PERMEABILITY TO CO_2 AND HCO_3^- IN THE MARINE HAPTOPHYTES *EMILIANIA HUXLEYI* AND *CALCIDISCUS LEPTOPORUS* (PRYMNESIOPHYCEAE)[1]

Sonia Blanco-Ameijeiras, Heather M. Stoll

Department of Earth Sciences, ETH Zurich, Sonnegstrasse 5, Zurich 8092, Switzerland

Hongrui Zhang

Department of Earth Sciences, ETH Zurich, Sonnegstrasse 5, Zurich 8092, Switzerland
State Key Laboratory of Marine Geology, Tongji University, Shanghai, China

and Brian M. Hopkinson[2]

Department of Marine Sciences, University of Georgia, Athens, Georgia 30602, USA

Membrane permeabilities to CO_2 and HCO_3^- constrain the function of CO_2 concentrating mechanisms that algae use to supply inorganic carbon for photosynthesis. In diatoms and green algae, plasma membranes are moderately to highly permeable to CO_2 but effectively impermeable to HCO_3^-. Here, CO_2 and HCO_3^- membrane permeabilities were measured using an ^{18}O-exchange technique on two species of haptophyte algae, *Emiliania huxleyi* and *Calcidiscus leptoporus*, which showed that the plasma membranes of these species are also highly permeable to CO_2 (0.006–0.02 cm $\cdot$ s^{-1}) but minimally permeable to HCO_3^-. Increased temperature and CO_2 generally increased CO_2 membrane permeabilities in both species, possibly due to changes in lipid composition or CO_2 channel proteins. Changes in CO_2 membrane permeabilities showed no association with the density of calcium carbonate coccoliths surrounding the cell, which could potentially impede passage of compounds. Haptophyte plasma-membrane permeabilities to CO_2 were somewhat lower than those of diatoms but generally higher than membrane permeabilities of green algae. One caveat of these measurements is that the model used to interpret ^{18}O-exchange data assumes that carbonic anhydrase, which catalyzes ^{18}O-exchange, is homogeneously distributed in the cell. The implications of this assumption were tested using a two-compartment model with an inhomogeneous distribution of carbonic anhydrase to simulate ^{18}O-exchange data and then inferring plasma-membrane CO_2 permeabilities from the simulated data. This analysis showed that the inferred plasma-membrane CO_2 permeabilities are minimal estimates but should be quite accurate under most conditions.

Key index words: **carbon concentrating mechanism; CO_2; haptophyte; membrane; permeability**

***Abbreviations*: AQP, aquaporin; CA, carbonic anhydrase; CCM, carbon concentrating mechanism; DIC, dissolved inorganic carbon; FA, fatty acids; MIMS, membrane inlet mass spectrometry; PIC, particulate inorganic carbon**

Marine phytoplankton are highly diverse and include cyanobacteria and eukaryotic members from distinct, deeply diverged evolutionary lineages (Falkowski et al. 2004). When these lineages diverged, oceanic CO_2 concentrations were sufficiently high to saturate carbon fixation rates by RuBisCO, the slow, low-affinity yet ubiquitous enzyme that catalyzes entry of CO_2 into the Calvin cycle (Raven 1991, Tcherkez et al. 2006). However, CO_2 concentrations subsequently declined driving evolution of CO_2 concentrating mechanisms (CCMs) that work to elevate the concentration of CO_2 around RuBisCO accelerating CO_2 fixation rates (Raven et al. 2011, 2012). CCMs appear to have evolved independently in many phytoplankton lineages and likely have different functional architectures. Despite this, nearly all CCMs employ two primary components: bicarbonate transporters and carbonic anhydrases (Reinfelder 2011). CCMs must operate under the biophysical constraints imposed by lipid membranes, namely that small, uncharged molecules like CO_2 easily pass through lipid bilayers, whereas lipid bilayers block passage of charged molecules like HCO_3^-.

In eukaryotic phytoplankton, the structure and molecular components of the CCM have been most well studied in the model diatom, *Phaeodactylum tricornutum*, providing an example of how CCMs function (Hopkinson et al. 2016, Matsuda et al. 2017). *Phaeodactylum tricornutum* actively imports

[1]Received 30 January 2020. Revised 28 March 2020. First Published Online 17 May 2020.
[2]Author for correspondence: e-mail bmhopkin@uga.edu.
Editorial Responsibility: J. Raven (Associate Editor)

bicarbonate into the cell via membrane-embedded transporters and CO_2 passively diffuses into the cell through membranes. The inward CO_2 gradient is driven by active export of HCO_3^- from the cytoplasm and into the chloroplast, combined with the action of intracellular carbonic anhydrase that works to equilibrate CO_2 and HCO_3^- (Hopkinson et al. 2011). Once in the chloroplast, HCO_3^- is transported into the acidic thylakoid membranes, apparently being directed to the portion of the thylakoid that penetrates the pyrenoid, a proteinaceous compartment where the bulk of cellular RuBisCO is located. A carbonic anhydrase in this pyrenoid-penetrating thylakoid catalyzes the conversion of HCO_3^- to CO_2, which then diffuses out into the pyrenoid where it is fixed by RuBisCO (Kikutani et al. 2016). Confinement of RuBisCO to a discrete compartment is necessary to maintain an efficient CCM, since CO_2 easily diffuses through membranes. While the details of CCM function are likely different in other phytoplankton, the CCM of *P. tricornutum* illustrates the complicated interplay between DIC forms (CO_2 and HCO_3^-) as interconverted by CA, diffusive and active fluxes, and spatial segregation that combine to form a functional, efficient CCM.

Haptophyte CCMs are not as well understood as those of diatoms or cyanobacteria, due in part to the lack of a genetic manipulation system. However, physiological and genetic studies of haptophyte CCMs, primarily in the coccolithophore *Emiliania huxleyi*, have shown they acquire both CO_2 and HCO_3^- from the environment (Rost et al. 2003) and possess carbonic anhydrase to facilitate DIC processing (Elzenga et al. 2000, Rost et al. 2003, Soto et al. 2006). Many haptophytes have a pyrenoid where the bulk of carbon fixation presumably takes place using RuBisCOs with generally lower K_ms (~15–24 μM CO_2) than diatoms (Heureux et al. 2017). These characteristics indicate haptophytes do not need to elevate internal CO_2 concentrations as high as diatoms do to saturate photosynthesis. Despite this, photosynthesis is often not fully saturated with DIC at ambient CO_2, suggesting that haptophytes may operate weak CCMs (Reinfelder 2011). Coccolithophores, a type of haptophyte, also must acquire and process DIC to build the coccoliths that cover their exterior. It is unclear to what extent carbon acquisition and processing for photosynthesis and calcification are coupled in coccolithophores. Although there has long been speculation that CO_2 is produced by calcification and used to support photosynthesis, there has been little experimental evidence that support this (Monteiro et al. 2016).

Since CCMs orchestrate DIC flows in phytoplankton cells, they have an important influence on the ^{13}C isotopic composition of fixed carbon. The ^{13}C signature of bulk organic matter and individual constituents are important archives used to help interpret modern and paleo-oceanic conditions including CO_2 concentrations (Bidigare et al. 1999, Pagani 2014). Consequently, a better understanding of CCMs has been sought for paleo-oceanographic considerations.

CCM structure is closely linked to the permeability of membranes to CO_2 and HCO_3^-. Because CO_2 is a small, uncharged molecule, it easily passes through membranes (Gutknecht et al. 1977, Missner et al. 2008), though the exact permeability of membranes to CO_2 can be modified by lipid composition and CO_2 channels such as certain aquaporins (Endeward et al. 2014). The ability to passively move through membranes makes diffusive influx of CO_2 an energetically cheap way to acquire CO_2, but creates challenges for the CCM's ultimate purpose of concentrating CO_2 around RuBisCO. To minimize diffusive loss of CO_2, RuBisCO is often confined to a small compartment (the pyrenoid or carboxysome), which in the case of cyanobacteria is covered in a protein shell and resists passive CO_2 efflux (Rae et al. 2013, Turmo et al. 2017). In contrast, HCO_3^- is charged and so cannot passively diffuse through membranes. HCO_3^- transit across membranes requires an active transporter (Romero et al. 2004, Parker and Boron 2013), expending energy, but a positive aspect of this inability to pass through membranes is that high concentrations of HCO_3^- can be built up in the cell. High concentrations of HCO_3^- can then be equilibrated with CO_2 in confined spaces via CA to generate high CO_2 concentrations, as occurs in cyanobacterial and eukaryotic CCMs (Raven 1997, Price et al. 2008, Kikutani et al. 2016).

The overall permeability of cellular membranes to CO_2 and HCO_3^- can be affected by both the membrane's protein and lipid composition. Lipid bilayers are generally highly permeable to CO_2, but high cholesterol content has been shown to substantially reduce CO_2 permeability in animal membranes (Itel et al. 2012). Although somewhat controversial, it appears that some transmembrane channels, primarily certain aquaporins, facilitate CO_2 diffusion through membranes (Verkman 2002, Endeward et al. 2014). A tobacco aquaporin (AQP1) has been shown to increase membrane permeability to CO_2 in vitro and repression of this aquaporin reduced stomatal conductance indicating it helps supply CO_2 for photosynthesis (Uehlein et al. 2003). Similarly, over-expression of a diatom aquaporin led to increased CO_2 permeability of the plasma membrane suggesting the protein helps facilitate CO_2 influx for carbon fixation (Matsui et al. 2018).

The permeability of phytoplankton membranes to CO_2 and HCO_3^- has been measured in several species of diatoms and green algae (Tu et al. 1986, Sültemeyer and Rinast 1996, Hopkinson et al. 2011), but has not yet been directly measured in any haptophyte taxa. Here we report direct measurements of plasma-membrane permeability to CO_2 and HCO_3^- in two species of haptophytes, the coccolithophores *Emiliania huxleyi* and *Calcidiscus*

leptoporus. The effects of varying temperature and CO_2 on membrane permeabilities are also assessed.

MATERIALS AND METHODS

Experimental organisms and culture conditions. Two commonly occurring marine coccolithophores were obtained from the Roscoff Culture Collection: *Emiliania huxleyi* RCC1258 (a pelagic strain isolated off the Portuguese coast in 1998) and *Calcidiscus leptoporus* RCC 1130 (a pelagic strain isolated off the South Africa coast in 2000). Cultures were maintained in enriched natural seawater media prepared from 0.2 μm filtered natural seawater (Acropak filtration cartridge), amended with Aquil nutrients, trace metals, and vitamins (Price et al. 1988), and sterilized by autoclaving. Incubations were performed in 1L polycarbonate bottles at both 14 and 22°C in temperature controlled, lighted incubators (Percival Scientific) equipped with cool white fluorescent tubes (Alto II™ Technology), where photosynthetically active radiation (PAR) was 220 ± 32 μmol photons · m^{-2} · s^{-1} under a 14:10 h light:dark cycle. *Emiliania huxleyi* and *C. leptoporus* are cosmopolitan species found under a wide range of environments conditions. The temperatures and light levels employed here are within those commonly experienced in these species' natural habitats (Renaud et al. 2002, Read et al. 2013).

The seawater carbonate system was manipulated through continuous bubbling with air/CO_2 mixtures of either 1,000 or 150 ppm CO_2, without direct modification of culture dissolved inorganic carbon (DIC) or alkalinity conditions. Culture media was bubbled for at least 12 h before cell inoculation. To ensure that bubbling was sufficient to achieve equilibrium between the bubbled air/CO_2 and the media DIC systems, culture pH was measured on the total hydrogen ion scale using Thymol Blue (Zhang and Byrne, 1996) and compared with expected values for equilibrium. All pH values reported are on the total hydrogen ion scale for use in seawater DIC calculations (Zeebe and Wolf-Gladrow 2001). Initial and final DIC concentrations were also measured for all cultures. DIC concentrations were measured using a membrane inlet mass spectrometer (MIMS; PFEIFFER Vacuum) by acidifying 0.2 μm filtered (Millipore syringe filter unit) media samples to pH ~4.5 using 20 mM of citric acid buffer and making 4 standard additions of 500 μM DIC.

Cells were acclimated to experimental CO_2 manipulations at 14°C for at least eight generations and were acclimated to 22°C for at least five generations in diluted semi-continuous batch cultures (cell density was maintained below 70,000 cell · mL^{-1} for *Emiliania huxleyi* and 15,000 cells · mL^{-1} for *Calcidiscus leptoporus*). After acclimation, three biological replicates of experimental cultures were incubated for each species at target environmental conditions as described above, and cells were harvested in the exponential growth phase. Culture densities and sizes were tracked daily using a Beckman Coulter Z2 Coulter Particle Counter and Size Analyzer. Presence of unwanted prokaryotes and eukaryotes was not detected in the cultures during routine examination using a light microscope (OLYMPUS BH-2).

Membrane permeabilities. Membrane permeabilities to CO_2 and HCO_3^- were measured with an ^{18}O-exchange method using MIMS (Tu et al. 1978, Hopkinson et al. 2011). In this approach, DIC is labeled with ^{18}O, which is gradually exchanged for ^{16}O in water as CO_2/HCO_3^- undergo hydration/dehydration cycles. The enzyme carbonic anhydrase (CA) catalyzes CO_2 hydration/HCO_3^- dehydration and so accelerates the rate of ^{18}O-exchange. Cells typically contain intracellular CA, which can only be accessed by extracellular CO_2 and HCO_3^- (and so accelerate ^{18}O removal) if these species can pass through the membranes separating internal CA from extracellular ^{18}O-labeled DIC. Assays are conducted in the dark to minimize active inorganic carbon transport.

The time course of ^{18}O removal is monitored by MIMS and CO_2 and HCO_3^- membrane permeabilities can be determined by quantitative analysis of this data. Details of the model used to interpret the data are found in Hopkinson et al. (2011), but key features of the model are that it treats the inside of the cell as a single homogeneous compartment containing CA, separated from external, labeled ^{18}O-DIC by a membrane as illustrated in Figure 1. All fluxes are treated as first order with respect to CO_2/HCO_3^- concentrations. The rate constants describing CO_2 and HCO_3^- fluxes into the cell (cellular transfer coefficients: f_c, f_b) include the effects of (a) transfer through the diffusive boundary layer ($f_{c\text{-DBL}}$, $f_{b\text{-DBL}}$) and (b) transfer through the membranes separating CA from the external environment ($f_{c\text{-m}}$, $f_{b\text{-m}}$). The effect of the diffusive boundary layer can be calculated assuming the cell is spherical (Pasciak and Gavis 1974):

$$f_{\mathrm{DBL}} = 4\pi RD$$

where R is the radius of the cell and D is the diffusion coefficient for either CO_2 (to calculate $f_{c\text{-DBL}}$), or HCO_3^- (to calculate $f_{b\text{-DBL}}$).

Knowing $f_{c\text{-DBL}}$ and $f_{b\text{-DBL}}$, the membrane permeability can then be determined by considering the overall cellular transfer coefficient as the result of two transfer processes in series:

$$\frac{1}{f_c} = \frac{1}{f_{c-\mathrm{DBL}}} + \frac{1}{f_{c-\mathrm{m}}}$$

$$\mathrm{P_c} = \frac{f_{c-\mathrm{m}}}{A}$$

where P_c is the membrane permeability to CO_2 and A is the cell surface area (Hopkinson et al. 2011). Analogous equations can be used to calculate the membrane permeability to HCO_3^-.

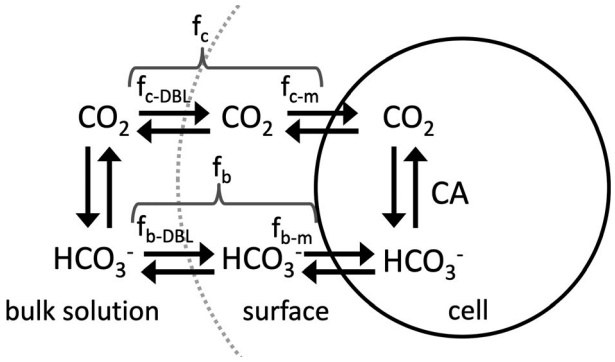

FIG. 1. Diagram of the model used to interpret ^{18}O-exchange data. ^{18}O-labeled CO_2 and HCO_3^- in the bulk solution (monitored by MIMS) must first pass through the cell's diffusive boundary layer to the cell surface ($f_{c\text{-DBL}}$, $f_{b\text{-DBL}}$). Then, CO_2 and HCO_3^- must pass through the cell membrane ($f_{c\text{-m}}$, $f_{b\text{-m}}$) to enter the cell where carbonic anhydrase is present, accelerating ^{18}O-exchange with ^{16}O in water. The combined effect these two processes (f_c, f_b) can be measured by quantitative analysis of ^{18}O-exchange data.

To conduct the ^{18}O-exchange assay, the chamber of the MIMS was loaded with assay buffer consisting of DIC-free artificial seawater with 20 mM Tris buffer matching the pH of the culture conditions (pH 7.78 for 1,000 ppm CO_2 cultures and pH 8.26 for 150 ppm CO_2 cultures). 2 mM ^{18}O-,^{13}C- DIC (98% ^{13}C, 97% ^{18}O) was added to the chamber and allowed to undergo uncatalyzed hydration/dehydration for ~10 min to determine the background rate of hydration/dehydration. Although preliminary experiments indicated these coccolithophore species expressed little to no extracellular CA, 50 μM dextran-bound acetazolamide (DBAZ) was added as an extra precaution to inhibit any extracellular CA activity. An aliquot of the experimental cultures was concentrated by gentle (<5 in Hg) vacuum filtration onto a 3 μm polycarbonate membrane filter (Whatman Cyclopore), resuspended in assay buffer, and a portion of the cell suspension was added to the MIMS chamber after the 10 min background period. ^{18}O-exchange in the presence of cells was then monitored for ~15 min. The cell density was calculated using a Beckman Coulter Z2.

Particulate inorganic carbon. The particulate inorganic carbon (PIC) content of selected coccolithophore cultures was determined by measuring acid-labile Ca^{2+} and assuming it was derived from $CaCO_3$. A 50 mL aliquot of culture was gently filtered (<5 in Hg) onto a 3 μm polycarbonate membrane filter (Whatman Cyclopore) and stored at −20°C. The filters were then immersed in 2 mL of 2% nitric acid for 24 h to dissolve $CaCO_3$ and the nitric acid was collected. The concentration of Ca^{2+} retained in the nitric acid was measured using Inductively Coupled Plasma Mass Spectrometry (Agilent 8800 ICP-QQQ-MS). Culture cell numbers and size were determined using a Coulter Counter Z2 and PIC content was normalized to cell number or surface area.

Two-compartment simulation. A two-compartment model was used to generate simulated ^{18}O-exchange data to assess the potential effects of subcellular compartments (chloroplast, mitochondrion) on inferred plasma-membrane CO_2 permeabilities. As diagrammed in Figure 2, the model consists of the bulk solution, an outer compartment, and an inner compartment. Both the compartments contain CA, potentially with different activities (outer: k_{cf}; inner: $k_{cf\text{-}x}$), and transfers between the bulk solution and the outer compartment are controlled by transfer coefficients (f_c, f_b), as are transfers between the outer and inner compartments ($f_{c\text{-}x}$, $f_{b\text{-}x}$). The size, surface area, and plasma-membrane permeabilities for CO_2 and HCO_3^- were set to typical values measured for *Emiliania huxleyi*. The inner compartment's HCO_3^- transfer coefficient ($f_{b\text{-}x}$) was set to a constant low value (1×10^{-12} $cm^3 \cdot s^{-1}$) based on results presented below showing that plasma-membrane HCO_3^- permeabilities are very low or indistinguishable from zero. k_{cf} was varied from low values to values typically measured in *Emiliania huxleyi*. $f_{c\text{-}x}$ and $k_{cf\text{-}x}$ were varied over several orders of magnitude covering all relevant possibilities. The ^{18}O-exchange data simulated using this model was then analyzed using the standard one-compartment model to infer plasma-membrane permeabilities to CO_2 and HCO_3^- (Tu et al. 1978, Hopkinson et al. 2011).

RESULTS

Culture DIC conditions. As shown in Table 1, target pH/CO_2 concentrations were generally achieved, although the low CO_2 treatments' pH did not quite reach target values. Nonetheless, there was clear separation between treatments and DIC conditions were maintained throughout the culture period.

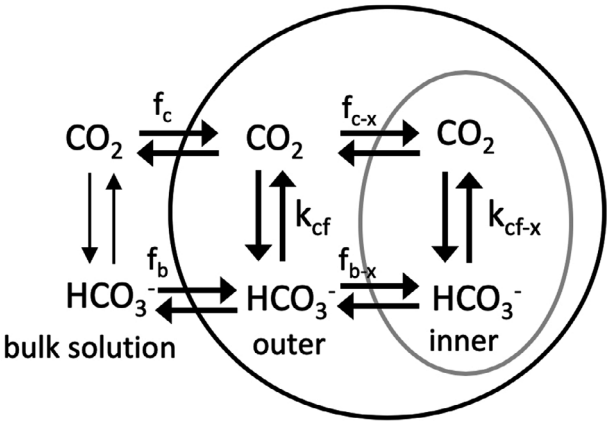

FIG. 2. Diagram of two-compartment model used to assess the effects of an inhomogeneous CA distribution on inferred plasma-membrane CO_2 permeabilities.

Membrane permeabilities. ^{18}O-exchange experiments were conducted to assess the permeability of haptophyte membranes to CO_2 and HCO_3^-. These experiments were conducted in the dark to minimize active inorganic carbon transport and isolate the effects of passive fluxes across membranes allowing inference of membrane permeabilities. Analysis of ^{18}O-exchange data showed that the one-compartment model was able to fit the data well (Fig. 3). However, a few samples were removed due to poor model fit, generally when cell numbers or CA activity were low leading to minimal acceleration of ^{18}O removal after cell addition. A total of 47 samples were analyzed to determine membrane permeabilities among the two species and four treatments (n = 3–10).

Cellular CO_2 transfer coefficients (f_c) were significantly affected by species ANOVA, $F_{3,43} = 18.5$, ($P < 1 \times 10^{-4}$), temperature (ANOVA, $F_{3,43} = 24.6$, $P < 1 \times 10^{-4}$), and CO_2 treatment (ANOVA, $F_{3,43} = 5.3$, $P < 0.05$) as determined by one-way analysis of variance (ANOVA). Post-hoc Tukey HSD tests (Fig. 4A) confirmed that f_c for *Calcidiscus leptoporus* was generally higher than that of *Emiliania huxleyi,* and that *C. leptoporus* had especially high f_c in the high temperature and high CO_2 treatment.

Membrane permeabilities (P_c) were significantly affected by temperature (ANOVA, $F_{4,42} = 19.5$, $P < 1 \times 10^{-3}$) and CO_2 treatment (ANOVA, $F_{4,42} = 7.8$, $P < 0.05$), and there was a significant interaction between temperature and CO_2 (ANOVA, $F_{4,42} = 0.01$, $P < 0.05$) as determined by ANOVA analysis. In contrast to f_c, membrane permeabilities were not significantly different between species ($P > 0.05$; Fig. 4B).

Cellular HCO_3^- transfer coefficients (f_b) and membrane permeabilities (P_b) were near or below the limit of detection for the method. Model parameters (including f_b) are determined through optimization of the model fit to ^{18}O-exchange data. As

TABLE 1. Culture DIC conditions. Reported values are means ± standard deviations. pH_{exp}: expected pH given CO_2 treatment; t0: initial culture conditions; tf: final culture conditions

Treatments			pH		DIC (mM)		CO_2 (μM)	
CO_2 (ppm)	Temp (°C)	pH_{exp}	t0	tf	t0	tf	t0	tf
150	14	8.39	8.26 ± 0.02	8.26 ± 0.03	1.90 ± 0.24	1.90 ± 0.02	8.3 ± 1.3	8.2 ± 0.6
1,000	14	7.69	7.85 ± 0.16	7.64 ± 0.08	2.46 ± 0.06	2.19 ± 0.19	25.0 ± 8.7	35.7 ± 3.8
150	22	8.37	8.26 ± 0.02	8.26 ± 0.03	1.91 ± 0.17	1.87 ± 0.08	5.9 ± 0.7	8.1 ± 1.9
1,000	22	7.69	7.75 ± 0.07	7.69 ± 0.03	2.21 ± 0.14	2.10 ± 0.08	33.6 ± 4.0	36.4 ± 2.2
150	14	8.39	8.32 ± 0.01	8.24 ± 0.00	1.94 ± 0.05	2.04 ± 0.19	7.1 ± 0.3	9.3 ± 0.8
1,000	14	7.69	7.68 ± 0.13	7.59 ± 0.10	2.24 ± 0.34	2.22 ± 0.04	39.8 ± 5.7	49.1 ± 12.0
150	22	8.37	8.31 ± 0.07	8.28 ± 0.04	1.80 ± 0.12	1.91 ± 0.03	5.4 ± 0.2	6.6 ± 2.6
1,000	22	7.69	7.70 ± 0.07	7.55 ± 0.04	2.42 ± 0.03	2.61 ± 0.07	34.6 ± 5.7	53.0 ± 5.6

part of this procedure, the error in model parameters for each sample is estimated through the extent to which changing the model parameter away from the best fit value increases model-data error. The errors in individual determinations of f_b were often larger than the value of f_b, indicating that its value was not significantly different from zero, and in all cases these errors were a substantial fraction of f_b, averaging 170 ± 470%. In contrast, fitting errors for f_c averaged 5.4 ± 4.5%. Consequently, the fitting errors were propagated to calculate the mean and standard deviations for f_b and P_b as shown in Figure 5. For most treatments, the mean of f_b and P_b was not significantly different from zero and in all cases f_b and P_b are ~1,000-fold lower than f_c and P_c. No further statistical analyses were conducted because in many cases samples converged to extremely similar, low f_b values, an artifact of optimization. Conducting statistical analyses on these artifactually similar values would give misleading results.

Particulate inorganic carbon. PIC per cell was significantly affected by species (ANOVA, $F_{4,17} = 22.5$, $P < 0.001$) and CO_2 (ANOVA, $F_{4,17} = 5.3$, $P < 0.05$) as determined by ANOVA analysis. However, post-hoc Tukey HSD tests showed differences between species were most notable among individual treatments with PIC per cell being higher in the larger *Calcidiscus leptoporus* (Fig. 6). PIC per unit surface area was not significantly affected by species, CO_2, or temperature as determined by ANOVA analysis.

Two-compartment model simulations. To assess the implications of a potentially inhomogeneous distribution of CA inside the cell, a two-compartment model, containing different CA activities in each compartment, was developed and used to simulate ^{18}O-exchange data (Fig. 2). The simulated ^{18}O-exchange data were then analyzed with the one-compartment model (Fig. 1) that is used to analyze actual data. Inferred membrane permeabilities were compared with values used in the simulation. In the two-compartment model, the outer compartment represents the plasma membrane and cytosol, and the second compartment, contained within the outer compartment, represents a subcellular compartment such as the chloroplast or mitochondrion.

Comparison of the inferred plasma-membrane CO_2 permeability with the value imposed in the simulation shows that the inferred permeability represents a minimal estimate of the actual value (Fig. 7). In the simulations, the imposed plasma-membrane permeability (outer compartment) was held constant at 0.09 cm · s^{-1}, in the middle of the measured range, while the inner compartment's CA activity ($k_{cf\text{-}x}$) and transfer coefficient ($f_{c\text{-}x}$) were varied systematically. The transfer coefficient combines surface area and membrane permeability ($f_{c\text{-}x} = P_{c\text{-}x} \times SA_x$); therefore, variation in this parameter can be interpreted as reflecting changes in either component.

Simulations were run at four different CA activities for the outer compartment (k_{cf} = 50–400 · s^{-1}). The inferred plasma-membrane CO_2 permeability is accurately recovered, with some noise due to optimization vagaries, when CA activity is high in the outer compartment (Fig. 7C and D). Under these circumstances, most of the ^{18}O-label is removed within the outer compartment, masking the inner compartment. Even when the outer compartment's CA activity is low, the presence of the inner compartment only alters the inferred plasma-membrane permeability when the CA activity of the inner compartment ($k_{cf\text{-}x}$) is high and when the transfer coefficient of the inner compartment ($f_{c\text{-}x}$) is moderately lower than the transfer coefficient of the outer compartment (Fig. 7A and B). When $f_{c\text{-}x}$ is very low, the inner compartment is effectively closed off and not accessible to ^{18}O-labeled DIC. Conversely, when $f_{c\text{-}x}$ is much higher than the outer compartment's transfer coefficient (f_c), exchange between the inner and outer compartment is fast relative to exchange between the outer compartment and the bulk solution and so the two compartments are effectively one. In this case, the permeability of the less permeable membrane, the outer membrane, is recovered by the one-compartment model fit. Only when $f_{c\text{-}x}$ is comparable to f_c do the two compartments interact, and the one-compartment fit is detecting a mixture of the outer and inner compartment membrane permeabilities. Nonetheless, the inferred plasma-membrane permeability is always a minimal estimate and under the range of parameters tested the

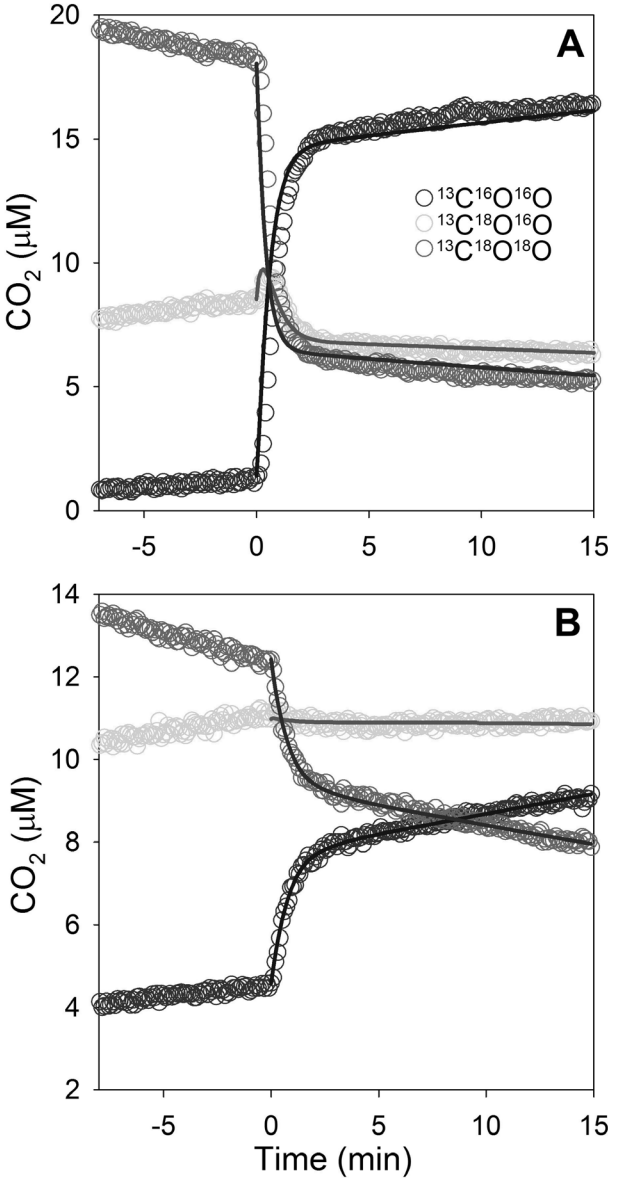

FIG. 3. Examples of ^{18}O-exchange data/model agreement in (A) *Emiliania huxleyi* and (B) *Calcidiscus leptoporus*. Circles represent data points and lines are the model fit after addition of cells at $t = 0$.

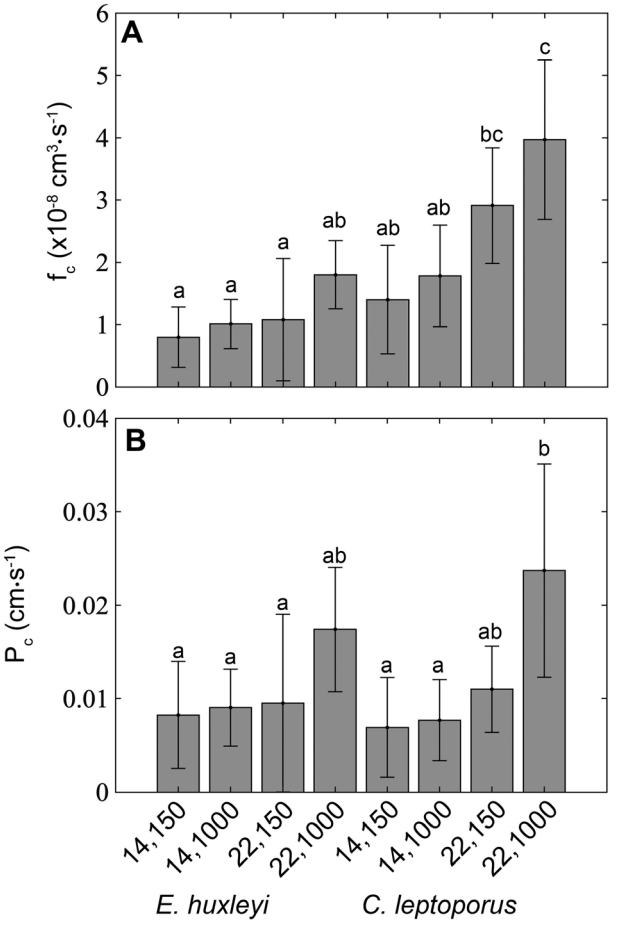

FIG. 4. (A) Cellular CO_2 mass transfer coefficients and (B) CO_2 membrane permeabilities. The labels on the *x*-axis indicate temperature (14 or 22°C) and CO_2 (150 or 1,000 ppm) treatments. Treatments with significantly different means, as assessed with a Tukey HSD test, are labeled with a different letter.

inferred permeability was at worst half that of the actual permeability.

DISCUSSION

Membrane permeabilities to CO_2 and HCO_3^- are an important constraint on CCM function and affect the carbon isotope composition of organic matter, a widely used paleo-oceanographic tracer. However, there have been few determinations of CO_2 and HCO_3^- membrane permeabilities in algae and none from haptophyte algae. To determine plasma-membrane permeabilities, we used an ^{18}O-exchange method in which intracellular CA rapidly removes ^{18}O-label from DIC. In order for ^{18}O-labeled DIC to encounter CA, it must pass through intervening biological membranes such that the extent of ^{18}O removal in the bulk solution provides a measure of membrane permeability. The model used to analyze ^{18}O-exchange data assumes that the cell is a spherical, homogeneous compartment surrounded by a single membrane (Fig. 1) and though the model fits data from both species well (Fig. 3), it is worth examining these assumptions. The assumption that the cell is spherical is quite a good approximation for the coccolithophore species examined here, with the caveat that they are coated in coccoliths forming a "coccosphere" surrounding the cell. The potential effect of the coccosphere on inferred membrane permeability will be discussed below. However, it is unlikely that CA is homogeneously distributed inside the cell. Localization of CAs in coccolithophores has been hindered by lack of a genetic manipulation system, but in other

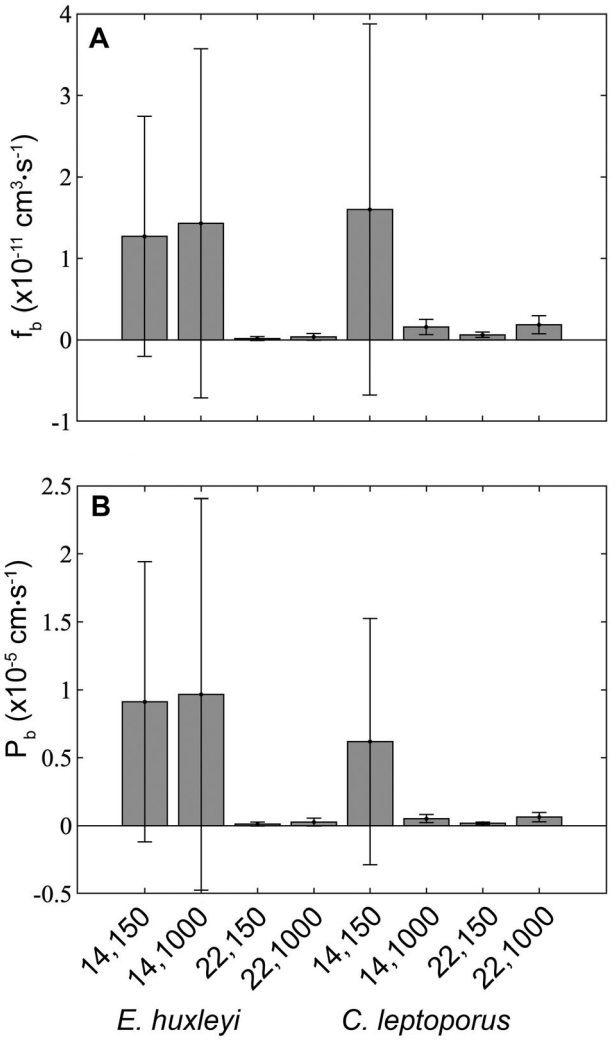

FIG. 5. (A) Cellular HCO_3^- mass transfer coefficients and (B) HCO_3^- membrane permeabilities. The labels on the x-axis indicate temperature (14 or 22°C) and CO_2 (150 or 1,000 ppm) treatments.

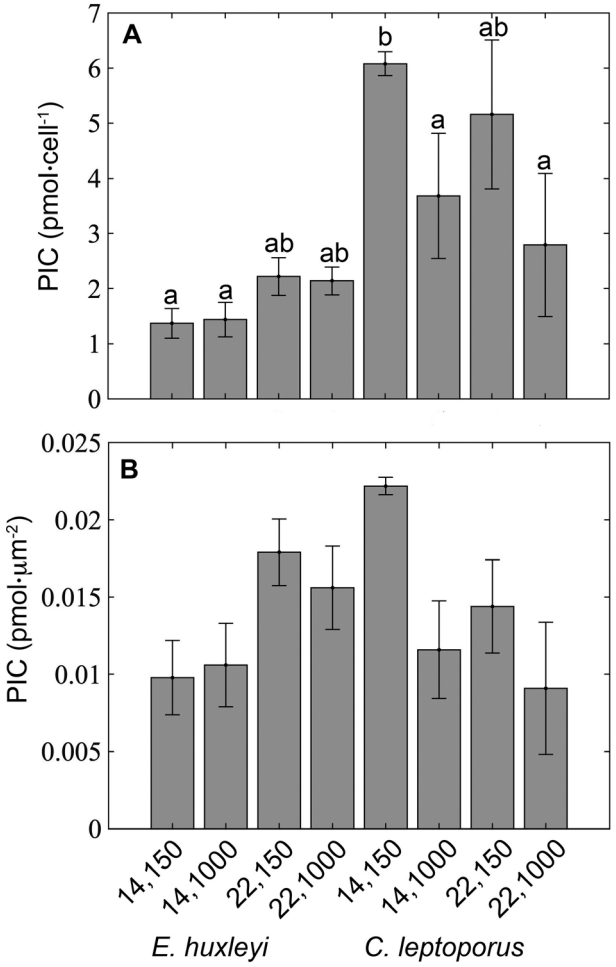

FIG. 6. (A) PIC per cell and (B) PIC/SA. The labels on the x-axis indicate temperature (14 or 22°C) and CO_2 (150 or 1,000 ppm) treatments.

algae, such as diatoms and green algae, CAs are found in diverse compartments including the cytoplasm, chloroplast, and periplastidal compartment (Moroney et al. 2011, Matsuda et al. 2017). Consequently, the ^{18}O-exchange signal likely integrates the effects of multiple intracellular CAs separated from external, ^{18}O-labeled DIC by a variable number of membranes (plasma, chloroplast, thylakoid, etc.).

The effects of inhomogeneous CA distribution on inferred plasma-membrane CO_2 permeabilities were explored by simulating ^{18}O-exchange data in a model in which intracellular CA was differentially distributed between two compartments and analyzing the simulated data using the standard model that assumes a homogeneous distribution of CA. This analysis showed that the inferred plasma-membrane permeabilities are minimum estimates, but they should be correct within approximately a factor of two given that we explored a wide parameter space (Fig. 7). It should be emphasized that this analysis considers the effect of inhomogeneous distribution of intracellular CA, as opposed to extracellular or periplasmic CA, on inferred membrane permeabilities. The presence of extracellular CA makes it extremely difficult to infer membrane permeabilities using the ^{18}O-exchange method, which is why an extracellular CA inhibitor (DBAZ) was applied in the experiments.

We measured CO_2 cellular transfer coefficients and plasma-membrane permeabilities in two coccolithophore species with significantly different cell size, *Emiliania huxleyi* (6.6 ± 0.4 µm diameter) and *Calcidiscus leptoporus* (9.1 ± 0.8 µm diameter). Analysis of the ^{18}O-exchange data leads directly to determination of the CO_2 cellular transfer coefficient (f_c), a per cell measure of CO_2 accessibility. This parameter can be useful: given f_c and the CO_2 concentration the gross CO_2 flux into the cell can be calculated. However, it is difficult to compare these

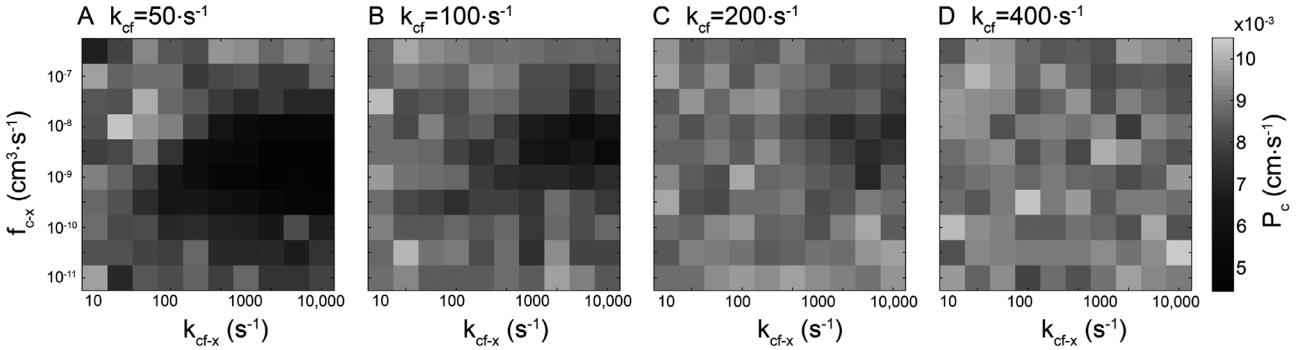

FIG. 7. Plasma-membrane CO_2 permeabilities inferred from simulated ^{18}O-exchange data from a two-compartment model with inhomogeneous CA distribution. The actual CO_2 permeability of the plasma membrane in the two-compartment model is 9×10^{-3} cm · s^{-1}.

values between species since larger cells will inherently have larger f_c values. Unsurprisingly, f_c was larger in the larger coccolithophore species, *C. leptoporus*, but more interestingly f_c was affected by both temperature and CO_2. f_c was especially large at high CO_2 and high temperature. Extracting plasma-membrane permeabilities from f_c requires normalization to cell surface area and accounting for the effect of the diffusive boundary layer on CO_2 transit from the bulk solution to the cell surface (Fig. 1; Pasciak and Gavis 1974). Accounting for the effects of the diffusive boundary layer is especially critical when membrane resistance to a compound is low, as is the case for CO_2. For these coccolithophore species, the diffusive boundary layer resistance accounted for 22 ± 11% of the overall resistance to CO_2 flux. CO_2 membrane permeabilities in both species were ~ 0.006 – 0.02 cm · s^{-1} and were significantly higher at elevated CO_2 and temperature, but there were no differences between species. These values are somewhat lower than permeabilities measured in diatoms, but approximately one order of magnitude higher than in green algae (Table 2).

CO_2 membrane permeabilities can be affected by the lipid composition of the membrane and by proteins embedded in the lipid membrane. The classic model for permeability of pure lipid membranes considers the membrane as a planar sheet of thickness Δx through which a compound must diffuse at a rate determined by the diffusion coefficient, D_m, and in which a compound may be enriched or depleted relative to the bulk solution, represented by the partition coefficient, K_p (Missner and Pohl 2009). In which case:

$$P_m = \frac{D_m K_p}{\Delta x}$$

For a given compound, membrane permeability is thought to be most affected by changes in D_m resulting from changes in the lipid composition that alter membrane fluidity, with more fluid membranes having higher D_m. Membrane thickness does not vary greatly and K_p is less affected by changes in lipid composition (Gutknecht et al. 1977). Artificial lipid bilayers are highly permeable to CO_2 (0.35–3.2 cm · s^{-1}; Gutknecht et al. 1977, Missner et al. 2008) and it was long assumed that biological membranes would also be extremely permeable to CO_2. However, recent work, especially on human cells, has indicated that the intrinsic permeability of biological membranes is often lower (Endeward et al. 2014), most likely due to differences in lipid composition between artificial lipid bilayers and biological ones. High cholesterol content of animal membranes in particular has been identified as potential factor reducing the diffusivity of CO_2 by reducing membrane fluidity (Itel et al. 2012). For example, the intrinsic membrane permeability of several human cell types appears to be ~ 0.01 cm · s^{-1}, much lower than artificial lipid bilayers but quite similar to the membrane permeabilities of

TABLE 2. Comparison of algal membrane permeabilities to CO_2

Species	Taxa	P_c (cm · s^{-1})	Source
Emiliania huxleyi	Cocco	$1.0 \pm 0.5 \times 10^{-2}$	This study
Calcidiscus leptoporus	Cocco	$1.2 \pm 0.8 \times 10^{-2}$	This study
Phaeodactylum tricornutum	Diatom	$3.1 \pm 0.4 \times 10^{-2}$	Hopkinson et al. (2011)
Thalassiosira weissflogii	Diatom	$2.4 \pm 0.7 \times 10^{-2}$	Hopkinson et al. (2011)
Thalassiosira pseudonana	Diatom	$5.6 \pm 1.1 \times 10^{-2}$	Hopkinson et al. (2011)
Thalassiosira oceanica	Diatom	$1.5 \pm 0.2 \times 10^{-2}$	Hopkinson et al. (2011)
Chlorella vulgaris	Green Algae	8.6×10^{-5}	Tu et al. (1986)
Chlamydomonas reinhardtii	Green Algae	$1.3 \pm 0.4 \times 10^{-3}$	Sültemeyer and Rinast (1996)

coccolithophores determined as part of this study and diatoms.

Membrane fluidity is highly sensitive to temperature and compensating modifications to lipid composition are commonly made to maintain membrane fluidity. Membrane lipids in algae, as in many other organisms (Hazel 1995), often shift toward longer-chain, more saturated forms at higher temperatures in an apparent attempt to maintain a constant membrane fluidity (Hu et al. 2008, Pittera et al. 2014). However, some microalgae such as diatom *Thalassiosira pseudonana* show more complex changes in fatty acid (FA) composition, with decreased chain length and decreased saturation in response to higher temperature (O'Donnell et al. 2019). Haptophyte membranes were more permeable to CO_2 at higher temperature (22°C) than at lower temperature (14°C; Fig. 4), which could be explained either by an increase in membrane fluidity that was not fully compensated for by changes in lipid composition or a direct consequence of changes in lipid composition. We are aware of no published study of coccolithophore FA changes in response to temperature. CO_2 concentrations can also affect membrane lipid composition of algae, though the functional significance of this is not well understood. In several algal species, very high CO_2 concentrations (2%) led to more saturated membrane lipids (Pronina et al. 1998, Sato et al. 2003), which would be expected to decrease membrane fluidity and permeability, opposite to the increased membrane permeability at high CO_2 found in *Emiliania huxleyi* and *Calcidiscus leptoporus*. In *E. huxleyi*, an increase in CO_2 from 1 to 15 μM was accompanied by an increase in the degree of saturation of FA but a decrease in average chain length (Riebesell et al. 2000). If the decrease in average chain length observed in that *E. huxleyi* study was representative, it could contribute to increased membrane fluidity and permeability.

Proteins embedded in biological membranes, such as channels and pores, can also alter membrane permeability to compounds. For CO_2, certain aquaporins and Rh proteins increase membrane permeability to CO_2 (Nakhoul et al. 1998, Endeward et al. 2008). Aquaporins are most commonly known as transmembrane water channels that help regulate water flow through plant tissues (Chaumont and Tyerman 2014), but this large protein family has members that facilitate transmembrane fluxes of other small molecules including glycerol, ammonia, urea, and CO_2 (Loque et al. 2005, Gomes et al. 2009). The Rh protein RhAG has been definitely shown to function as an ammonia channel (Ripoche et al. 2004), but it and other homologs may also function as CO_2 channels, including in algae such as *Chlamydomonas reinhardtii* (Soupene et al. 2002, Endeward et al. 2008). The coccolithophores studied here generally had higher membrane permeabilities to CO_2 when cultured under high CO_2 conditions (Fig. 4). Consistent with this pattern, a CO_2 permeating aquaporin in the diatom *Thalassiosira pseudonana* was up-regulated at high CO_2 and the Rh homolog in *C. reinhardtii* was up-regulated at high CO_2 (Soupene et al. 2002, Matsui et al. 2018). *Emiliania huxleyi* has at least six AQP homologs (Matsui et al. 2018), so up-regulation of a CO_2 permeating AQP is a potential explanation for increased membrane CO_2 permeability at high CO_2, though no haptophyte AQPs have yet been functionally characterized. One AQP, AQP2, was assessed in *E. huxleyi* in high and low CO_2 treatments and showed no significant transcriptional response (Bach et al. 2013). However, other AQPs, which were not assessed, may contribute to CO_2 permeability. CO_2 uptake becomes an increasingly important fraction of total DIC uptake for photosynthesis for *E. huxleyi* and other eukaryotic marine phytoplankton as CO_2 concentrations increase and pH decreases (Rost et al. 2003, Kottmeier et al. 2016). An increased membrane permeability may help facilitate the increased CO_2 transmembrane flux under high CO_2, low pH conditions.

The estimated CO_2 membrane permeabilities include any barriers to CO_2 flux other than the diffusive boundary layer, which was explicitly accounted for (Fig. 1). Coccolithophores are surrounded by a coccosphere of calcium carbonate coccoliths, which could potentially impede CO_2 flux and affect observed membrane permeabilities. To assess this possibility, we determined the PIC content per unit surface area (PIC_{SA}) of coccolithophores (Fig. 6B) and used a linear model to examine effects on membrane permeabilities. PIC_{SA} was not significantly affected ($P > 0.05$) by temperature (ANOVA, $F_{4,42} = 0.1$), or CO_2, variables that affected CO_2 membrane permeability, and so we treated PIC_{SA} as an additional independent variable in a linear model to explain variation in membrane permeability. PIC_{SA} did not have a significant effect on membrane permeability (ANOVA, $F_{3,18} = 0.3$, $P = 0.61$), suggesting the coccosphere does not substantially impede CO_2 diffusion. The coccosphere is composed of loosely assembled coccoliths, which frequently shed, and so it is likely that the gaps between coccoliths and openings between coccolith elements provide sufficient space for diffusion of compounds to the cell surface. Even diatoms, whose structurally rigid, nanoporous silica shell might be expected to present a more substantial barrier to diffusion than the coccosphere, have high observed membrane permeabilities to CO_2 (Hopkinson et al. 2011). Although the coccoliths do not appear to affect CO_2 diffusion, it is possible that they alter CCM function in other ways. For example, the calcium carbonate could serve as proton buffer for external CA as has been demonstrated for the silica frustule of diatoms (Milligan and Morel 2002).

The membrane permeability to CO_2 also influences the fractionation between the isotopic

composition of the ambient $CO_{2\text{-aq}}$ and photosynthetically fixed organic carbon (ε_p). Because this fractionation (hereafter, ε_p) is from theory expected to correlate with the ratio of CO_2 supply to C demand via cell growth (Rau et al. 1996), it has been employed to estimate both algal growth rates in the ocean (Bidigare et al. 1999) as well as to estimate atmospheric CO_2 in the past (Pagani 2014). Cell membrane permeability sets the diffusive CO_2 supply into the cell. However, if carbon acquisition in coccolithophores were dominated by diffusive CO_2 uptake with limited significance of active HCO_3^- transport to the site of photosynthesis, as interpreted from some data (Rost et al. 2003), then the ε_p observed in culture experiments would require a 100-fold increase in cell membrane permeability in low CO_2 cultures to explain the maintenance of modest, rather than very low, ε_p (Stoll et al. 2019). The results from the first direct permeability measurements of *Emiliania huxleyi* reported here provide no evidence for such large variations in permeability, and suggest that permeability may be lower, rather than higher, under low CO_2 treatments. Consequently, purely diffusive models of coccolithophore carbon supply may not provide a robust quantitative description of ε_p. On the other hand, the task of modeling ε_p in multi-component cell models which simulate a CCM is simplified by the ability to assume only very limited variations in membrane permeability. Likewise, the limited variation in membrane permeability among two coccolithophore species in different experimental conditions, and the similarity of coccolithophore and diatom membrane permeabilities, suggests that it may be robust to assume that ancient strains of coccolithophores had similar membrane permeabilities to their modern relatives. This latter assumption will also simplify efforts to estimate past atmospheric pCO_2 from determinations of ε_p in fossil algal biomarkers.

HCO_3^- membrane permeabilities were near or below the detection limit for the ^{18}O-exchange method ($\leq \sim 1 \times 10^{-5}$ cm $\cdot$ s^{-1}), approximately three orders of magnitude lower than CO_2 permeabilities. Extremely low HCO_3^- membrane permeabilities, in many cases indistinguishable from zero, were also found in four species of diatom and green algae suggesting this is a common feature among algae (Tu et al. 1986, Hopkinson et al. 2011). Charged species are generally not able to cross lipid bilayers without protein pores, channels, or transporters. Algae do have active transport mechanisms for HCO_3^- to support photosynthetic needs (Nakajima et al. 2013, Wang et al. 2015), but these are not active in the dark when the ^{18}O-exchange assays are conducted.

Here, we showed that the plasma membranes of two coccolithophores are permeable to CO_2, as expected for a small, uncharged molecule, but nearly impermeable to HCO_3^-. CO_2 membrane permeabilities increased by at most ~ threefold under high CO_2, high temperature conditions, but did not change by orders of magnitude, as has been suggested in some models to explain variation in carbon isotopic fractionation of photosynthetically produced organic matter assuming solely diffusive acquisition of CO_2. Simulations showed that inferred plasma-membrane CO_2 permeabilities may be modestly affected (at most twofold) by the internal distribution of CA when cytoplasmic CA activity is low and CA activity in other subcellular compartments is high. These new data provide context for better understanding the CO_2 concentrating mechanisms of haptophyte algae and the mechanism by which carbon isotopic values are imprinted on organic matter preserved in oceanic sediments.

This work was supported by the Swiss National Science Foundation (Award 200021_182070 to HMS) and ETH core funding, and the US National Science Foundation (OPP 1744760 to BMH). The authors are grateful to Kaylie Plumb for support with the maintenance of stock cultures and Madalina Jaggi for the ICP-MS analysis.

Bach, L. T., Mackinder, L., Schulz, K. G., Wheeler, G., Schroeder, D. C., Brownlee, C. & Riebesell, U. 2013. Dissecting the impact of CO_2 and pH on the mechanisms of photosynthesis and calcification in the coccolithophore *Emiliania huxleyi*. *New Phytol.* 199:121–34.

Bidigare, R. R., Hanson, K. L., Buesseler, K. O., Wakeham, S. G., Freeman, K. H., Pancost, R. D., Millero, F. J., Steinberg, P., Popp, B. N. & Latasa, M. 1999. Iron-stimulated changes in ^{13}C fractionation and export by equatorial Pacific phytoplankton: toward a paleogrowth rate proxy. *Paleoceanography* 14:589–95.

Chaumont, F. & Tyerman, S. D. 2014. Aquaporins: highly regulated channels controlling plant water relations. *Plant Physiol.* 164:1600–18.

Elzenga, J. T. M., Prins, H. B. A. & Stefels, J. 2000. The role of extracellular carbonic anhydrase activity in inorganic carbon utilization of Phaeocystis globose (Prymnesiophyceae): A comparison with other marine algae using the isotope disequilibrium technique. *Limnol. Oceanogr.* 45:372–380.

Endeward, V., Al-Samir, S., Itel, F. & Gros, G. 2014. How does carbon dioxide permeate cell membranes? A discussion of concepts, results and methods. *Front. Physiol.* 4:21.

Endeward, V., Cartron, J. P., Ripoche, P. & Gros, G. 2008. RhAG protein of the Rhesus complex is a CO_2 channel in the human red cell membrane. *Faseb J.* 22:64–73.

Falkowski, P. G., Katz, M. E., Knoll, A. H., Quigg, A., Raven, J. A., Schofield, O. & Taylor, F. J. R. 2004. The evolution of modern eukaryotic phytoplankton. *Science* 305:354–60.

Gomes, D., Agasse, A., Thiebaud, P., Delrot, S., Geros, H. & Chaumont, F. 2009. Aquaporins are multifunctional water and solute transporters highly divergent in living organisms. *Biochim. Biophys. Acta Biomembr.* 1788:1213–28.

Gutknecht, J., Bisson, M. & Tosteson, F. 1977. Diffusion of carbon dioxide through lipid bilayer membranes: effects of carbonic anhydrase, bicarbonate, and unstirred layers. *J. Gen. Physiol.* 69:779.

Hazel, J. R. 1995. Thermal adapation in biological membranes – is homeoviscous adaptation the explanation? *Ann. Rev. of Physiol.* 57:19–42.

Heureux, A. M. C., Young, J. N., Whitney, S. M., Eason-Hubbard, M. R., Lee, R. B. Y., Sharwood, R. E. & Rickaby, R. E. M. 2017. The role of RuBisCO kinetics and pyrenoid

morphology in shaping the CCM of haptophyte microalgae. *J. Exp. Botany* 68:3959–69.

Hopkinson, B. M., Dupont, C. L., Allen, A. E. & Morel, F. M. M. 2011. Efficiency of the CO_2-concentrating mechanism of diatoms. *Proc. Natl. Acad. Sci. USA* 108:3830–37.

Hopkinson, B. M., Dupont, C. L. & Matsuda, Y. 2016. The physiology and genetics of CO_2 concentrating mechanisms in model diatoms. *Curr. Opin. Plant Biol.* 31:51–57.

Hu, Q., Sommerfeld, M., Jarvis, E., Ghirardi, M., Posewitz, M., Seibert, M. & Darzins, A. 2008. Microalgal triacylglycerols as feedstocks for biofuel production: perspectives and advances. *Plant J.* 54:621–39.

Itel, F., Al-Samir, S., Oberg, F., Chami, M., Kumar, M., Supuran, C. T., Deen, P. M. T., Meier, W., Hedfalk, K., Gros, G. & Endeward, V. 2012. CO_2 permeability of cell membranes is regulated by membrane cholesterol and protein gas channels. *Faseb J.* 26:5182–91.

Kikutani, S., Nakajima, K., Nagasato, C., Tsuji, Y., Miyatake, A. & Matsuda, Y. 2016. Thylakoid luminal theta-carbonic anhydrase critical for growth and photosynthesis in the marine diatom *Phaeodactylum tricornutum*. *Proc. Natl. Acad. Sci. USA* 113:9828–33.

Kottmeier, D. M., Rokitta, S. D. & Rost, B. 2016. H^+-driven increase in CO_2 uptake and decrease in HCO_3^- uptake explain coccolithophores' acclimation responses to ocean acidification. *Limnol. Oceanogr.* 61:2045–57.

Loque, D., Ludewig, U., Yuan, L. X. & von Wiren, N. 2005. Tonoplast intrinsic proteins AtTIP2;1 and AtTIP2;3 facilitate NH3 transport into the vacuole. *Plant Physiol.* 137:671–80.

Matsuda, Y., Hopkinson, B. M., Nakajima, K., Dupont, C. L. & Tsuji, Y. 2017. Mechanisms of carbon dioxide acquisition and CO_2 sensing in marine diatoms: a gateway to carbon metabolism. *Philos. T. R. Soc. London, Ser. B* 372:12.

Matsui, H., Hopkinson, B. M., Nakajima, K. & Matsuda, Y. 2018. Plasma membrane-type aquaporins from marine diatoms function as CO_2/NH_3 channels and provide photoprotection. *Plant Physiol* 178:345–57.

Milligan, A. J. & Morel, F. M. M. 2002. A proton buffering role for silica in diatoms. *Science* 297:1848–50.

Missner, A., Kugler, P., Saparov, S. M., Sommer, K., Mathai, J. C., Zeidel, M. L. & Pohl, P. 2008. Carbon dioxide transport through membranes. *J. Biol. Chem.* 283:25340–47.

Missner, A. & Pohl, P. 2009. 110 years of the Meyer-Overton Rule: predicting membrane permeability of gases and other small compounds. *ChemPhysChem* 10:1405–14.

Monteiro, F. M., Bach, L. T., Brownlee, C., Brown, P., Rickaby, R. E. M., Poulton, A. J., Tyrrell, R. et al. 2016. Why marine phytoplankton calcify. *Sci. Adv.* 2:e1501822.

Moroney, J. V., Ma, Y. B., Frey, W. D., Fusilier, K. A., Pham, T. T., Simms, T. A., DiMario, R. J., Yang, J. & Mukherjee, B. 2011. The carbonic anhydrase isoforms of *Chlamydomonas reinhardtii*: intracellular location, expression, and physiological roles. *Photosyn. Res.* 109:133–49.

Nakajima, K., Tanaka, A. & Matsuda, Y. 2013. SLC4 family transporters in a marine diatom directly pump bicarbonate from seawater. *Proc. Natl. Acad. Sci. USA* 110:1767–72.

Nakhoul, N. L., Davis, B. A., Romero, M. F. & Boron, W. F. 1998. Effect of expressing the water channel aquaporin-1 on the CO_2 permeability of *Xenopus* oocytes. *Am. J. Physiol.* 274: C543–C548.

O'Donnell, D. R., Du, Z. Y. & Litchman, E. 2019. Experimental evolution of phytoplankton fatty acid thermal reaction norms. *Evol. Appl.* 12:1201–11.

Pagani, M. 2014. Biomarker-based inferences of past climate: The alkenone pCO_2 proxy. *In* Holland, H. & Turekian, K. [Eds.] *Treatise on Geochemistry*. Elsevier, Oxford, pp. 361–78.

Parker, M. D. & Boron, W. F. 2013. The divergence, actions, roles, and relatives of sodium-coupled bicarbonate transporters. *Physiol. Rev.* 93:803–959.

Pasciak, W. J. & Gavis, J. 1974. Transport limitation of nutrient uptake in phytoplankton. *Limnol. Oceanogr.* 19:881–98.

Pittera, J., Humily, F., Thorel, M., Grulois, D., Garczarek, L. & Six, C. 2014. Connecting thermal physiology and latitudinal niche partitioning in marine Synechococcus. *ISME J.* 8:1221–36.

Price, G. D., Badger, M. R., Woodger, F. J. & Long, B. M. 2008. Advances in understanding the cyanobacterial CO_2-concentrating-mechanism (CCM): functional components, C_i transporters, diversity, genetic regulation and prospects for engineering into plants. *J. Exp. Bot.* 59:1441–61.

Price, N. M., Harrison, G. I., Hering, J. G., Hudson, R. J., Nirel, P. M. V., Palenik, B. & Morel, F. M. M. 1988. Preparation and chemistry of the artificial algal culture medium Aquil. *Biol. Oceanogr.* 6:443–62.

Pronina, N. A., Rogova, N. B., Furnadzhieva, S. & Klyachko-Gurvich, G. L. 1998. Effect of CO_2 concentration on the fatty acid composition of lipids in *Chlamydomonas reinhardtii* cia-3, a mutant deficient in CO_2-concentrating mechanism. *Russ. J. Plant Physiol.* 45:447–55.

Rae, B. D., Long, B. M., Badger, M. R. & Price, G. D. 2013. Functions, compositions, and evolution of the two types of carboxysomes: polyhedral microcompartments that facilitate CO_2 fixation in cyanobacteria and some proteobacteria. *Microbiol. Mol. Biol. Rev.* 77:357–79.

Rau, G., Riebesell, U. & Wolf-Gladrow, D. 1996. A model of photosynthetic ^{13}C fractionation by marine phytoplankton based on diffusive molecular CO_2 uptake. *Mar. Ecol. Prog. Ser.* 133: 275–85.

Raven, J. A. 1991. Implications of inorganic carbon utilization – ecology, evolution and geochemistry. *Can. J. Bot. – Rev. Can. Bot.* 69:908–924.

Raven, J. A. 1997. CO_2 concentrating mechanisms: a direct role for thylakoid lumn acidification. *Plant Cell Env.* 20:147–154.

Raven, J. A., Giordano, M., Beardall, J. & Maberly, S. C. 2011. Algal and aquatic plant carbon concentrating mechanisms in relation to environmental change. *Photosyn. Res.* 109:281–96.

Raven, J. A., Giordano, M., Beardall, J. & Maberly, S. C. 2012. Algal evolution in relation to atmospheric CO_2: carboxylases, carbon-concentrating mechanisms and carbon oxidation cycles. *Philos. T. R. Soc. B* 367:493–507.

Read, B. A., Kegel, J., Klute, M. J., Kuo, A., Lefebvre, S. C., Maumus, F., Mayer, C. et al. 2013. Pan genome of the phytoplankton *Emiliania* underpins its global distribution. *Nature* 499:209–13.

Reinfelder, J. R. 2011. Carbon concentrating mechanisms in eukaryotic marine phytoplankton. *Ann. Rev. Mar. Sci.* 3:291–315.

Renaud, S., Ziveri, P. & Broerse, A. T. C. 2002. Geographical and seasonal differences in morphology and dynamics of the coccolithophore *Calcidiscus leptoporus*. *Mar. Micropaleontol.* 46:363–85.

Riebesell, U., Revill, A. T., Holdsworth, D. G. & Volkman, J. K. 2000. The effects of varying CO_2 concentration on lipid composition and carbon isotope fractionation in *Emiliania huxleyi*. *Geochim. Cosmochim. Acta* 64:4179–92.

Ripoche, P., Bertrand, O., Gane, P., Birkennmeier, C., Colin, Y. & Cartron, J. P. 2004. Human Rhesus-associated glycoprotein mediates facilitated transport of NH_3 into red blood cells. *Proc. Natl. Acad. Sci. USA* 101:17222–27.

Romero, M. F., Fulton, C. M. & Boron, W. F. 2004. The SLC4 family of HCO_3^- transporters. *Pflugers Arch.* 447:495–509.

Rost, B., Riebesell, U., Burkhardt, S. & Sültemeyer, D. 2003. Carbon acquisition of bloom-forming marine phytoplankton. *Limnol. Oceanogr.* 48:55–67.

Sato, N., Tsuzuki, M. & Kawaguchi, A. 2003. Glycerolipid synthesis in *Chlorella kessleri* 11h - II. Effect of the CO_2 concentration during growth. *Biochim. Biophys. Acta Mol. Cell Biol. Lipids* 1633:35–42.

Soto, A. R., Zheng, H., Shoemaker, D., Rodriguez, J., Read, B. A. & Wahlund, T. M. 2006. Identification and preliminary characterization of two cDNAs encoding unique carbonic anhydrases from the marine alga *Emiliania huxleyi*. *Appl. Environ. Microbiol.* 72:5500–11.

Soupene, E., King, N., Feild, E., Liu, P., Niyogi, K. K., Huang, C. H. & Kustu, S. 2002. Rhesus expression in a green alga is regulated by CO_2. *Proc. Natl. Acad. Sci. USA* 99:7769–73.

Stoll, H. M., Guitian, J., Hernandez-Almeida, I., Mejia, L. M., Phelps, S., Polissar, P., Rosenthal, Y., Zhang, H. & Ziveri, P. 2019. Upregulation of phytoplankton carbon concentrating

mechanisms during low CO_2 glacial periods and implications for the phytoplankton pCO_2 proxy. *Quat. Sci. Rev.* 208:1–20.

Sültemeyer, D. & Rinast, K. 1996. The CO_2 permeability of the plasma membrane of *Chlamydomonas reinhardtii*: mass-spectrometric ^{18}O-exchange measurements from $^{13}C^{18}O_2$ in suspensions of carbonic anhydrase-loaded plasma-membrane vesicles. *Planta* 200:358–68.

cherkez, G. G. B., Farquhar, G. D. & Andrews, T. J. 2006. Despite slow catalysis and confused substrate specificity, all ribulose bisphosphate carboxylases may be nearly perfectly optimized. *Proc. Natl. Acad. Sci. USA* 103:7246–51.

Tu, C. K., Acevedoduncan, M., Wynns, G. C. & Silverman, D. N. 1986. Oxygen-18 exchange as a measure of accessibility of CO_2 and HCO_3^- to carbonic anhydrase in *Chlorella vulgaris* (UTEX 263). *Plant Physiol.* 80:997–1001.

Tu, C., Wynns, G., McMurray, R. & Silverman, D. 1978. CO2 kinetics in red cell suspensions measured by 18O exchange. *J. Biol. Chem.* 253:8178–84.

Turmo, A., Gonzalez-Esquer, C. R. & Kerfeld, C. A. 2017. Carboxysomes: metabolic modules for CO_2 fixation. *FEMS Microbiol. Lett.* 364:7.

Uehlein, N., Lovisolo, C., Siefritz, F. & Kaldenhoff, R. 2003. The tobacco aquaporin NtAQP1 is a membrane CO_2 pore with physiological functions. *Nature* 425:734–37.

Verkman, A. S. 2002. Does aquaporin-1 pass gas? – an opposing view. *J. Physiol. Lond.* 542:31–31.

Wang, Y. J., Stessman, D. J. & Spalding, M. H. 2015. The CO_2 concentrating mechanism and photosynthetic carbon assimilation in limiting CO_2: how *Chlamydomonas* works against the gradient. *Plant J.* 82:429–48.

Zeebe, R. E. & Wolf-Gladrow, D. 2001. *CO_2 in Seawater: Equilibrium, Kinetics, Isotopes.* Elsevier, Amsterdam, 346 pp.

Zhang, H. N. & Byrne, R. H. 1996. Spectrophotometric pH measurements of surface seawater at in-situ conditions: absorbance and protonation behavior of thymol blue. *Mar. Chem.* 52:17–25.